Materials Science & Engineering A 585 (2013) 422–429

Contents lists available at ScienceDirect

Materials Science & Engineering A

journal homepage: www.elsevier.com/locate/msea

Impact–abrasion wear characteristics of in-situ VC-reinforced austenitic steel matrix composite

E.G. Moghaddam [a,*], N. Karimzadeh [b], N. Varahram [a], P. Davami [a]

[a] Department of Materials Science and Engineering, Sharif University of Technology, P.O. Box 11365-9466, Azadi Avenue, Tehran, Iran
[b] Department of Materials Engineering, Islamic Azad University, Najafabad Branch, Isfahan, Iran

ARTICLE INFO

Article history:
Received 14 April 2013
Received in revised form
19 July 2013
Accepted 31 July 2013
Available online 7 August 2013

Keywords:
Mechanical characterization
Austenite
Ferrous alloy
Casting
Fracture
Wear

ABSTRACT

In this investigation, in-situ precipitation of vanadium carbides was employed to reinforce Fe–13Mn and Fe–13Mn–3W alloys by means of conventional melting and casting route. Microstructures were characterized by optical and scanning electron microscopy techniques.

Mechanical properties of the materials were determined by hardness, impact toughness and tension tests. It was observed that tungsten improved the strength of the matrix and the reinforcements as well as tensile properties and work hardening rate of the VC-reinforced composite. Ball mill abrasion test was utilized to simulate impact–abrasion wear condition using two types of abrasive minerals. The results showed that the degree of benefit to be gained by the use of in-situ VC-reinforced composite materials depends strongly on crush strength of the abrasives. It was found that the studied particle-reinforced composite materials were only advantageous when the abrasives were relatively soft, providing low-stress abrasion condition.

1. Introduction

Wear is one of the three most commonly encountered industrial problems leading to the replacement of components and assemblies in engineering; the others being fatigue and corrosion. It can be broken down to five categories as: abrasive, adhesive, erosive, fretting and chemical wear. Among them, abrasive wear comprises roughly about 50% of industrial wear situations [1]. Abrasion is the wear process by which the surfaces of components are eroded by the gouging or scratching action of hard abrasives trapped between the contacting surfaces. It can be classified into various types according to the loading condition, the number of elements involved, the medium in which abrasion takes place etc. Impact–abrasion is characterized by the impact loading and the presence, in most cases, of three elements, i.e. the surfaces of two components and the abrasive particles [2].

Austenitic manganese steels (AMS) having a wide range of applications in cement and mineral processing industries are well known. Their most characteristic type contains 12–14 wt% manganese and 1.2–1.4 wt% carbon, which was invented in 1882 by Robert Hadfield and to this day, often is referred to as Hadfield steel [3,4]. This type of steel combines high toughness with ductility and high work-hardenability. It is therefore particularly useful for applications requiring resistance to impact–abrasion wear caused by rapid work-hardening [5,6].

However, austenitic manganese steel has certain properties that tend to restrict its use. It usually has a yield strength of only 345–415 MPa. Consequently, it is not well suited for parts that must resist plastic deformation when highly stressed in service [7]. Of many available and beneficial alloying additions to the AMS, it has been established that the curve for vanadium has the steepest slope in a graph of yield strength versus the percentage of alloying element [8]. In addition, a usual way to improve the abrasion resistance of a material is to raise its hardness which usually leads to reduction of toughness [9,10]. Generally, carbides in the microstructure depending on their type, morphology and volume fraction provide the hardness, which is required for applications without degradation [11]. Therefore, a new type of austenitic manganese steels was developed by the present researchers where its austenitic matrix was reinforced by in-situ precipitation of vanadium carbide particulates [12]. It was measured that the wear resistance of the in-situ VC-reinforced austenitic manganese steel matrix composite (V-AMS) was 5 times higher than that of the standard Hadfield steel under pin-on-disk abrasion test condition. On a continuing effort to improve the strength and wear resistance of austenitic manganese steels, tungsten was substituted with vanadium to certain quantities and the new steel group was investigated thoroughly [13]. It was observed that W has a beneficial effect on mechanical properties of the matrix. But, for a

* Corresponding author. Tel.: +98 911 291 7553; fax: +98 21 6600 5717.
E-mail addresses: emad_g_moghaddam@alum.sharif.edu, emad.g.moghaddam@gmail.com (E.G. Moghaddam).

0921-5093/$ - see front matter © 2013 Elsevier B.V. All rights reserved.
http://dx.doi.org/10.1016/j.msea.2013.07.082

fixed V+W addition of 10 wt%, tungsten contents above 2 wt% are detrimental for the wear resistance due to the formation of W_3C phase and the decrease in the volume fraction of the reinforcing VC particles.

As mentioned above, austenitic manganese steel parts are expected to perform best in impact load working conditions. On the other hand, the well-known pin-on-disk abrasion test cannot produce loading conditions of repeated impacts, although such conditions of loading are a very common feature of service applications [14]. In addition, field studies of the wear phenomena are time-consuming, expensive and difficult to control and/or quantify.

Ball mill abrasion test (BMAT) has not been standardized yet, but it has been recently used to reproduce the abrasive particle and counterbody kinematics as well as quantitative alloy performance comparisons closely matching those in impact–abrasion service conditions [15–17]. The purpose of the present study is to investigate the wear behavior V-AMS composite including an optimized tungsten-alloyed high-vanadium austenitic manganese steel composite (VW-AMS) subjected to impact–abrasion wear against quartz and hematite minerals using laboratory BMAT equipment.

2. Experimentals

Chemical composition of the unreinforced alloy and the composite materials are presented in Table 1. They were produced by remelting high manganese steel scraps in a medium frequency induction furnace. For the composite materials, low-carbon ferrovanadium and low-carbon ferrotungsten were added to the melts and maintained for 10 min at 1550–1580 °C. After complete dissolution of vanadium and tungsten, high-carbon ferromanganese and pure carbon were added at 1500 °C to adjust the chemical composition. After deoxidizing with 0.1% pure aluminum, the melts were poured in preheated ceramic molds at 1480–1520 °C and cooled to room temperature in air. Then, the castings were subjected to solution treatment at 1100 °C for 90 min followed by quenching in water. While austenitizing, to prevent surface decarburization, the samples were covered by cast iron chips in a sealed box. Tension test specimens were prepared according to ASTM A781. The tests were performed under strain rate control ($1.33 \times 10^{-3}\ s^{-1}$) at the room temperature. Tensile properties were measured as the average values obtained from five tensile tests. The coefficient of work hardening (n) was evaluated by using Hollomon's fitting equation [18]:

$$\text{Hollomon's equation}: \sigma = K\varepsilon^n \quad (1)$$

where σ stands for the true stress, ε is the true strain, K the strength coefficient and n is the strain hardening exponent of the material.

Metallographic samples were prepared according to conventional laboratory techniques. Five percent Nital solution was used to reveal the microstructures. The yellowish brown film was removed by immersion in a 15% solution of HCl in ethanol. The density of the materials was determined by Archimedes' method in distilled water, using an analytical balance equipped with a density measurement kit. The accuracy of the balance was 0.1 mg. XRD analysis was performed with Cu Kα radiation to identify the phase type with a Philips Xpert diffractometer. Microhardness of the matrices was measured using Vickers microhardness tester under applied load of 300 gr (HV0.3) for 15 s. Samples for Charpy unnotched impact test were also prepared as per ASTM E23. Ball mill abrasion test was carried out using a laboratory ball mill having a diameter of 700 mm rotating at 50 rpm. Two types of minerals were used to rank the performance of the studied materials; quartz sand as typical foundry sand (AFS 30 mesh) and hematite stone with mean diameter of 10–15 mm. For each set of test, the mill was charged with 20 kg of 17% chromium cast iron balls (10 kg of 50 mm diameter ball and 10 kg of 25 mm diameter ball)+7 kg of one of the above abrasives including 5 block-shaped specimens from each alloy composition. The specimens had dimensions typically 20 mm × 20 mm × 20 mm and weighted on average 80 gr each. A "wear-in" period of 15 h was conducted to remove surface defects coming from casting and heat treatment processes. Then, the specimens were marked and weighted with the balance before being exposed into the mill for the actual BMAT. Duration of ball mill test was 200 h. After each period of 20 h, the test was stopped temporarily; the specimens were retrieved, thoroughly cleaned and re-weighted to calculate the wear weight loss and then, the worn abrasives were replaced with fresh minerals for the next test period. Since, the studied materials had different densities; it was more accurate to use volumetric loss other than weight loss when comparing the amount of removed material from the specimens. Therefore, wear weight loss was converted to volume loss by using Eq. (2):

$$\text{Volumetric loss}\ (mm^3) = \frac{\text{Mass loss (g)}}{\text{Density}\ (g/mm^3)} \quad (2)$$

Table 1
Chemical composition of the materials (wt%).

Material	Fe	C	Mn	Si	Cr	V	W
AMS	Base	1.2	12.2	0.6	0.1	–	–
V-AMS	Base	2.9	13.1	0.5	0.3	10.1	–
VW-AMS	Base	3.0	12.9	0.7	0.3	9.1	3.0

3. Results and discussion

3.1. Microstructure

Fig. 1 shows optical microstructure of the standard Hadfield steel. The purpose of heat-treatment as such is to retain 100% austenite at room temperature with all the carbon dissolved in the matrix (Fig. 1b). However, the observed phase at grain boundary of the AMS is likely to be phosphide eutectics which are very common in solutionised-quenched Hadfield steels [19]. Microstructure of V-AMS composite is shown in Fig. 2a. It is composed of primary and secondary vanadium carbide particulates with reasonably uniform distribution in the matrix. The mechanism of the formation of VC particulates can be described as follows: initially, vanadium carbide phase forms during solidification through reaction of the solute vanadium with carbon in the molten steel. This leads to plentiful precipitation of coarse primary VC particles in the structure (about 20 vol%). With further reduction of temperature below solidus line, the solubility of vanadium and carbon in the Fe-γ decreases and secondary vanadium carbides appear in the matrix. These precipitates are very fine and have an average size of 150 nm, as shown in Fig. 2b. Fig. 2c shows the microstructure of VW-AMS composite. Similar to the former composite, solidification starts with nucleation and growth of vanadium carbide particles in the melt (about 20 vol%). With further reduction of temperature, solubility of tungsten in molten alloy decreases and an over-saturated solution is formed around solid particles. So, tungsten comes out from the melt and enters into the growing VC phase by substituting vanadium. This was confirmed by observation of a distribution gradient within VC particles of the VW-AMS composite. The EDS line-scanning across the VC particulate in Fig. 3 shows that concentration of tungsten increases whereas the concentration of vanadium decreases from core to periphery of the particle. Similar trend seems to be logical regarding secondary vanadium carbides. XRD analysis indicated that the matrix of the above composites was fully austenitic with V_8C_7 particulates

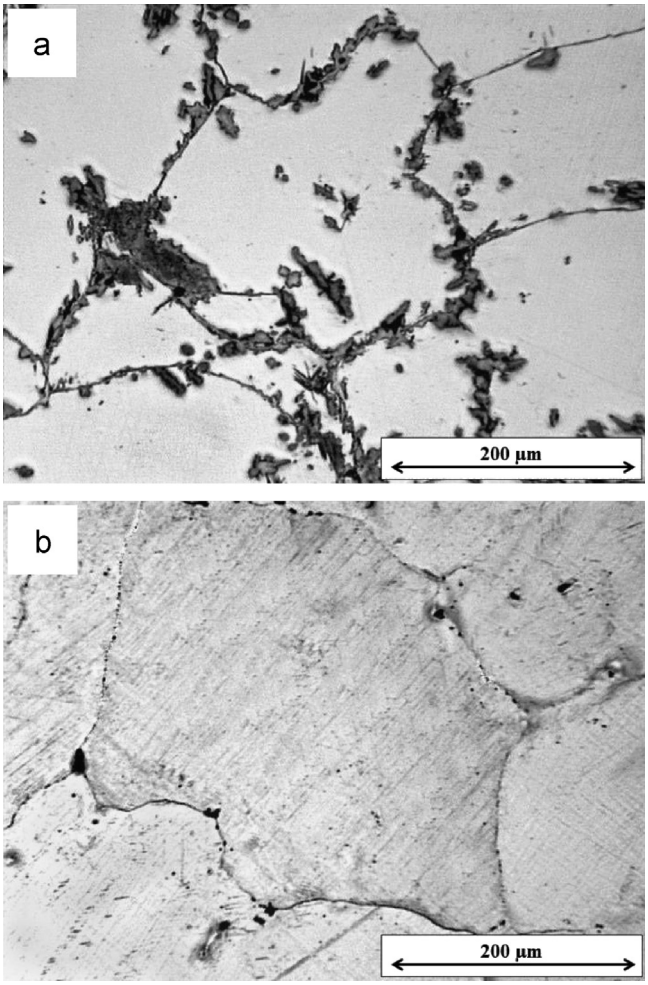

Fig. 1. Optical microstructure of AMS alloy: (a) as-cast condition and (b) heat-treated condition.

within the parent Fe lattice. In addition, no indication of tungsten carbide was observed in X-ray diffraction pattern of the VW-AMS material (Fig. 4).

3.2. Mechanical properties

Fig. 5 shows microhardness and impact toughness values of the AMS, V-AMS and VW-AMS materials. The higher hardness of the matrix in V-AMS composite compared to the conventional manganese steel can be related to dissolution of carbon and vanadium elements in Fe-γ lattice and also precipitation hardening effect of the fine secondary vanadium carbides. In addition, it can be seen that substitutional solution of tungsten provides extra hardening of the austenite in VW-AMS composite. This can be attributed to higher solubility of tungsten in austenite compared to vanadium [20] as well as larger difference in atomic radii between Fe and W in contrast to Fe and V atoms. The atomic radii of Fe, V and W are 126 pm, 134 pm and 139 pm, respectively [21]. Therefore, introducing tungsten into austenite creates higher local stress fields in iron crystal lattice leading to higher strength of the matrix. A similar effect of strengthening the primary vanadium carbides by tungsten dissolution was also observed in the W-alloyed composite as the average hardness of primary vanadium carbides in V-AMS and VW-AMS composites was 2650 HV and 2730 HV, respectively. However, compared to the unreinforced austenitic manganese steel, the composite materials showed much lower impact toughness. It may be the consequence of the brittle nature of vanadium carbides which reduced the plastic deformation capability of the matrix. In addition, the interface between the particulates and matrix is very prone to crack nucleation [22]. Thus, the cracks could easily form and propagate along the interface leading to failure of the composite.

Fig. 6 shows SEM micrograph of fractured surface of the composite materials. It is composed of cleavage facets indicating rapid fracture of the reinforcements deriving from their intrinsic brittleness and rigid structure. In addition, observation of some scattered dimples suggests ductile fracture of the austenite matrix similar to that of the conventional manganese steel [5]. In the presence of reinforcing particles, two major phenomena were distinguished in both studied composites; particle fracture and interfacial decohesion of the reinforcements (Fig. 6b and d) [23]. Basically, when the stress is applied, the matrix plastically deforms and gradually transfers the stress to the particles. The behavior of the particle depends on the relative strength between the interface and the matrix. When the load is transferred through the interface, fracture of reinforcement occurs as soon as the threshold stresses is reached [24]. Decohesion occurs when the average tensile stress in the particles surpasses a critical value known as the interface strength [23]. So, the higher impact toughness of VW-AMS could be explained according to the explained fracture mechanism and solidified structure of the composite materials. As mentioned above, primary vanadium carbides first formed in the melt during solidification. Then, tungsten atoms around VC particulates gradually dissolved into them through substitutional diffusion. This diffusion was likely to make the interface between the matrix and VC particles stronger in VW-AMS than that of the same in V-AMS composite as well as increasing the strength of the reinforcements themselves. Therefore, particle fracture and decohesion could be restrained by adding tungsten to V-AMS alloy. A similar effect has been reported by Srivastava and Das [25] where stronger reinforcement/matrix interface has been formed thorough diffusion of tungsten into TiC reinforcing particle acting as a barrier to reinforcement damage and decohesion.

Table 2 summarizes tensile properties of the investigated materials. Compared to the conventional austenitic manganese steel, the composite materials exhibited much higher yield and ultimate tensile strength. Apart from the undeniable effect of rigid second phase particles to withstand a portion of applied stress and reinforcing a typical composite, it is to be noted that, there is another key factor in regard to in-site reinforced composite materials which contributes to increase tensile properties. That is, the strengthening of the matrix via formation of a supersaturated solid solution by means of vanadium and tungsten in case of the present study. In fact, to enable the formation of in-situ reinforcing particles during solidification, the amount of participating elements was much higher than the solution limit of the parent matrix. The maximum solubility of vanadium and tungsten in an unalloyed Fe-γ is almost 1 wt% and 3 wt%, respectively [20]. This is far below the sum of the regarding elements in the present highly alloyed composite materials which resulted in higher strength of the matrix compared to that of the Hadfield steel. It has been reported in the literature that addition of only 2 wt% vanadium into the austenite increases the yield strength from about 370 MPa to more than 550 MPa [26]. A similar strengthening effect of tungsten in austenite has been recognized. However, the increase in ultimate tensile strength was predominant compared to the yield strength [27]. It can be observed that addition of 3 wt% tungsten in V-AMS composite has increased the yield and ultimate strength by 51 MPa and 94 MPa, respectively as well as ductility. So, the calculated area under the stress–strain curve of the tungsten-alloyed composite which is representative of the material toughness showed higher value despite the lower hardness of the matrix of V-AMS alloy. This could be related to the

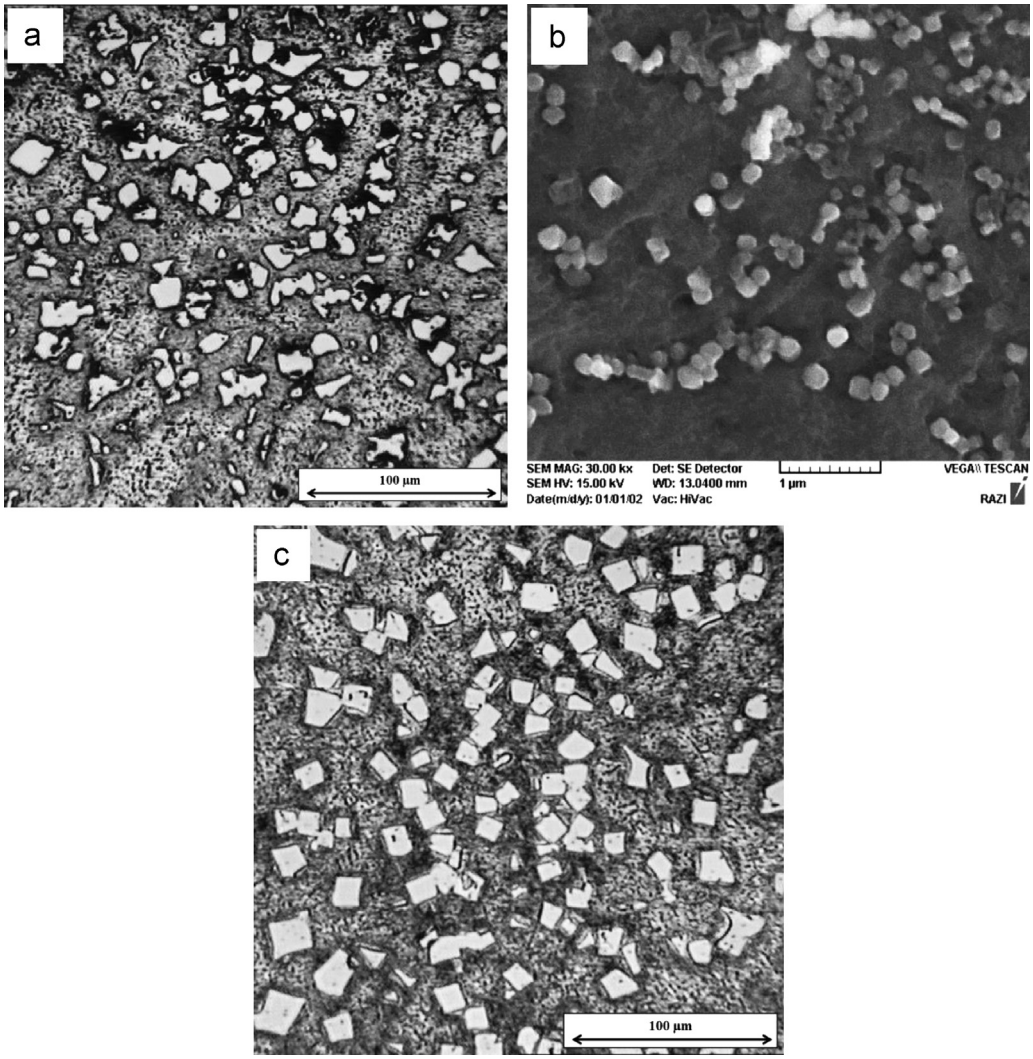

Fig. 2. Micrograph of: (a) V-AMS alloy, (b) secondary vanadium carbides and (c) VW-AMS alloy.

explained solidification mechanism of the VW-AMS composite which creates better interface bond of the matrix and particles [28].

3.3. Impact–abrasion wear resistance

Cumulative volume loss of the specimens as a function of milling time is shown in Fig. 7. The average mass loss of the specimens was found to be almost perfectly linear with the time. This suggests uniform material wear during ball milling. The wear situation occurring in ball mill grinding media is a combination of impact and abrasion interactions. Both these actions continually nip and remove certain quantities of material. According to the magnitude of impact and abrasion mechanisms in a ball mill charge profile, three zones of comminution actions can be defined as: grinding, tumbling and crushing zone. These zones are schematically shown in Fig. 8. In grinding zone, the wear mechanism is almost pure sliding, while the crushing zone is characterized by high-energy impacts. The situation in tumbling zone is moderate, including both sliding and low-energy impacts [29]. It has been reported that, combined impact–abrasion condition of ball milling would result in uniform removal of material and constant wear rate [16].

The coefficients of x in the linear equations shown in Fig. 7 represent the wear rates. It was observed that the unreinforced austenitic matrix steel exhibited poor resistance against the two abrasives. Material hardness relative to the hardness of the abrasives can be used as first indication to wear resistance. Experimentally, it has been shown that if the hardness of the abradant is at least 1.2 times that of the abraded surface, it can readily cause plastic deformation and accelerate material removal [10]. On the other hand, the metallic matrix of the present alloys is composed of austenite which is well known for its high work-hardenability. Therefore, a hardened layer is formed as soon as the surface of the specimens is subjected to mechanical wear [30]. This was demonstrated by the increase of the hardness of the matrix after the BMAT (Fig. 9). It is clear that all materials experience work-hardening due to the surface deformation of the austenite. Moreover, quartz work hardened the matrix to slightly higher extent than hematite in all cases which is indicative of severer surface interactions. For example, work hardening to approximately 480 HV and 525 HV was detected at the wear surface of the unreinforced austenite (Hadfield steel) in case of hematite and quartz, respectively. This corresponds to average 100% increase in hardness compared to the initial value. Consequently, instead of using initial hardness, the hardness of the worn/plastically deformed surface layer was considered when evaluating the wear resistance. However, in case of unreinforced austenitic matrix alloy, the hardness and yield strength were not high enough at the surface to withstand the plastic deformation imposed by the abrasives under the prevailing conditions of ball mill and wear rates were high.

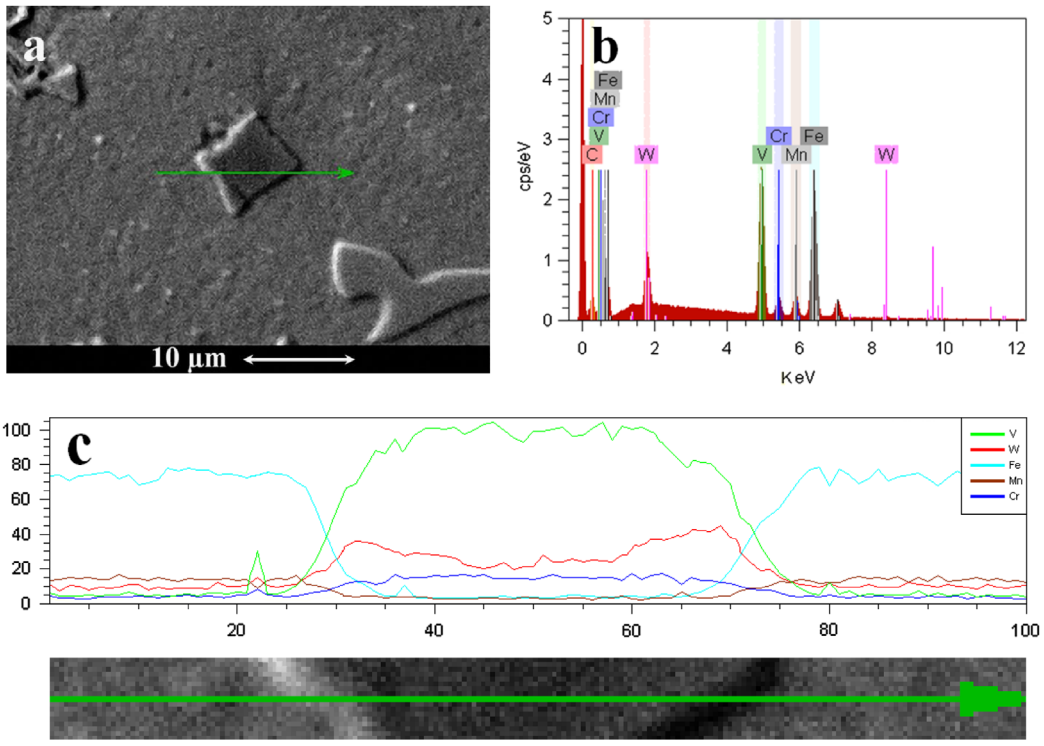

Fig. 3. (a) SEM micrograph, (b) EDX spectral analysis and (c) line-scan of a VC particulate in VW-AMS composite material.

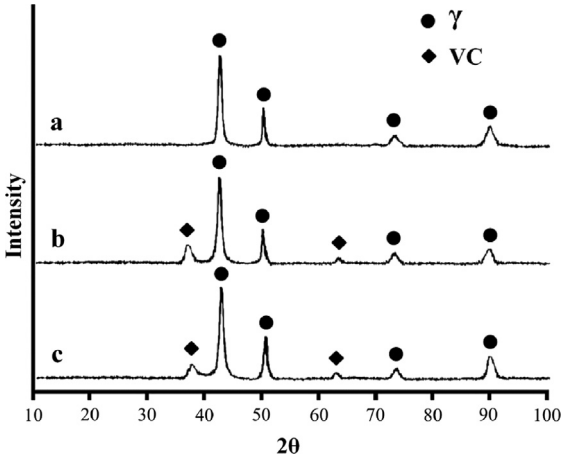

Fig. 4. XRD patterns of the experimental alloys: (a) AMS, (b) V-AMS and (c) VW-AMS.

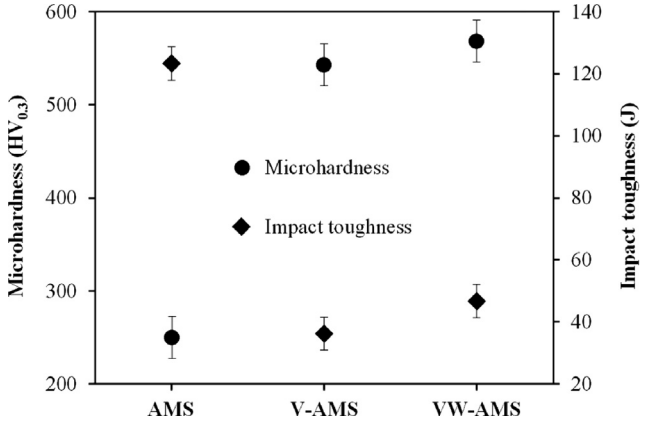

Fig. 5. Microhardness and impact toughness of the studied materials.

Compared to the conventional austenitic manganese steel, higher wear performance of the composite materials was due to the increase in mechanical properties of the austenite matrix such as initial hardness and yield strength which are prerequisite for satisfactory wear resistance in BMAT. Moreover, vanadium carbide particulates reduced the contact area of the matrix with abrasive particles and made the surface hard to plastic flow. Therefore, deformation and removal of the austenite by micro-cutting of the abradants was alleviated. It was observed that introducing tungsten to in-situ VC-reinforced composite was beneficial to the wear resistance. Specially, in case of hematite, nearly 45% improvement of wear life compared to V-AMS was distinguished.

To explain these results, the wear micromechanism of the composites was studied. Fig. 10 shows typical metallographic section perpendicular to the worn surface of the two composites. In addition to plastic deformation of the austenite, it could be observed that vanadium carbide particulates were damaged and fractured under impact loading condition during ball milling. In the present investigation, hematite (HV=580) and quartz (HV=1090) were adopted to be representative of a soft and a hard grinding media in BMAT. According to the above discussion, although vanadium carbides were too hard to be cut by hematite or even quartz grains due to their superior hardness, the severity of the interactions between the specimens with the charge (balls and abradants) was high enough to promote subsurface fatigue crack initiation and propagation in association with the reinforcements. The maximum depth of cracked carbides (D_{CC}) under the worn surface of composite specimens was observed until the depth of about 20 μm when quartz grains were used as abrasives. However, observation of this phenomenon was limited to not higher than 7 μm below the subsurface in case of hematite. In addition, surveying the cross section of specimens along the worn surface revealed that D_{CC} in case of quartz or hematite was averagely lower in VW-AMS compared to V-AMS in the same condition. It was suggested that the lower value of D_{CC} for the former composite in both of the above conditions was due to improved properties of the particulates and also the higher

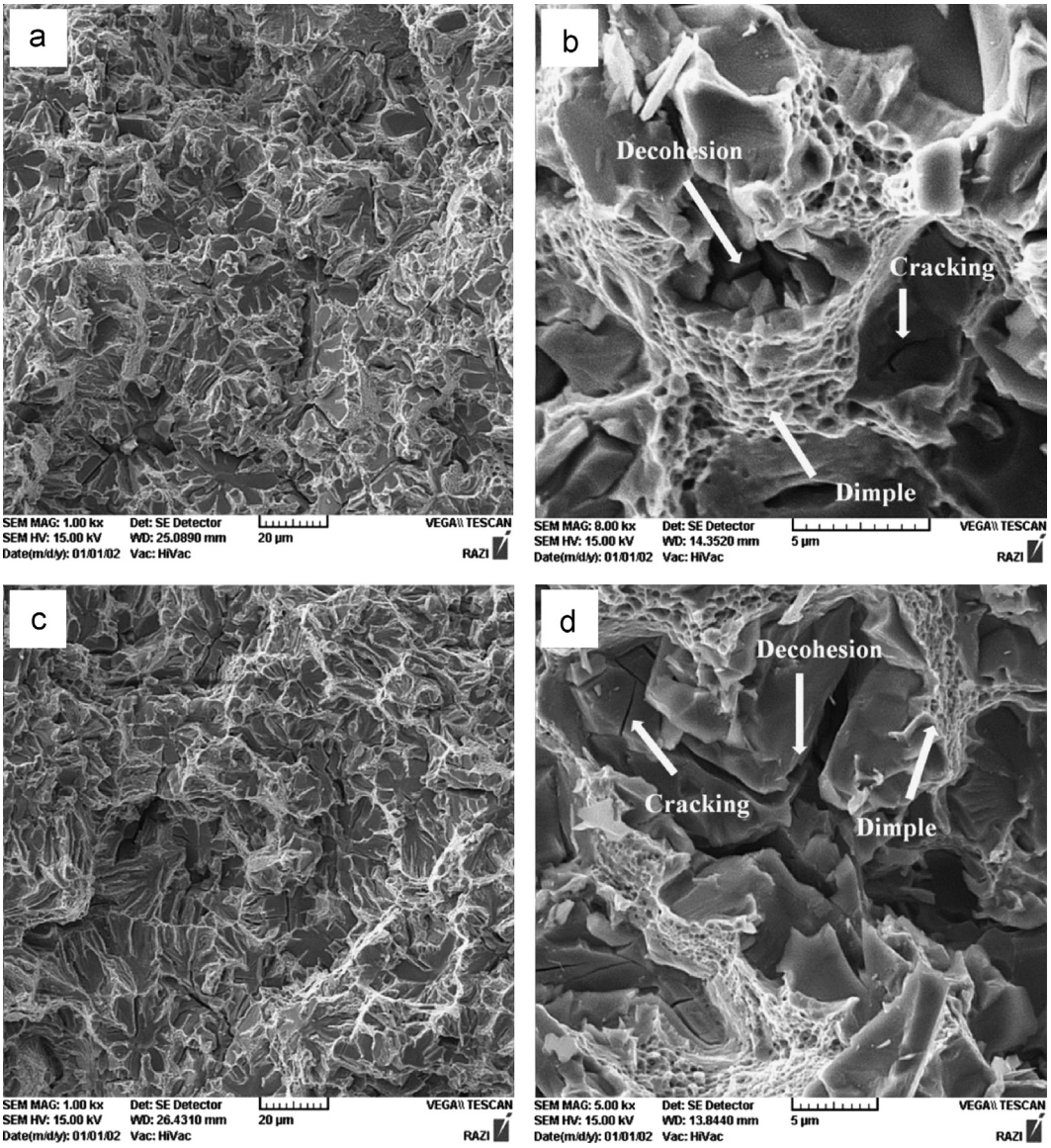

Fig. 6. Typical micrograph of fracture surface in; (a and b) V-AMS and (c and d) VW-AMS composite material.

Table 2
Tensile properties of the investigated materials.

Material	Yield strength (MPa)	Ultimate Strength (MPa)	Fracture strain	Strain hardening exponent	Specific work to fracture (J cm^{-3})
AMS	371	721	0.45	0.67	314
V-AMS	574	803	0.08	0.53	107
VW-AMS	625	897	0.11	0.56	148

strength of the matrix which could provide better support of the reinforcements. Observation of deeper microcracked reinforcements in case of quartz could be attributed to its stronger nature with respect to hematite. In fact, under the situation of BMAT with a soft mineral such as hematite, a considerable portion of the energy of collision between the involving components in wear process was consumed for comminution of the mineral grain itself. In other words, soft abrasives could act as bumper and cushion impactive loads of collisions. Therefore, less energy was left for crack formation and propagation in reinforcements. But, the situation with quartz was reversed as it could strongly resist

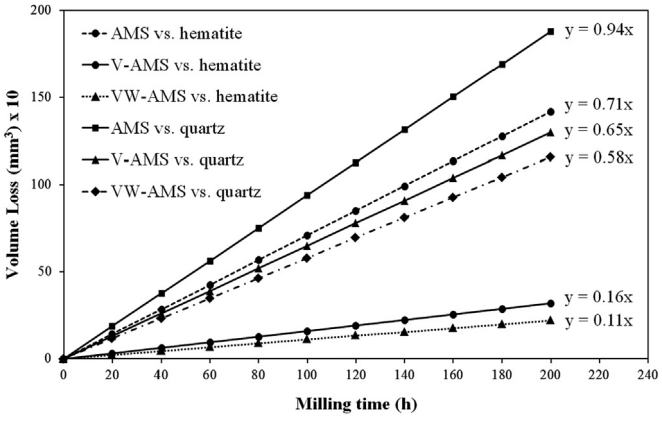

Fig. 7. Wear of investigated materials against hematite and quartz minerals in laboratory ball mill.

crushing and smashing when trapped between two mating bodies. Thus, a great amount of collision energy of the mill charge was transferred back to the composite specimens and caused deeper subsurface fatigue cracking of carbides.

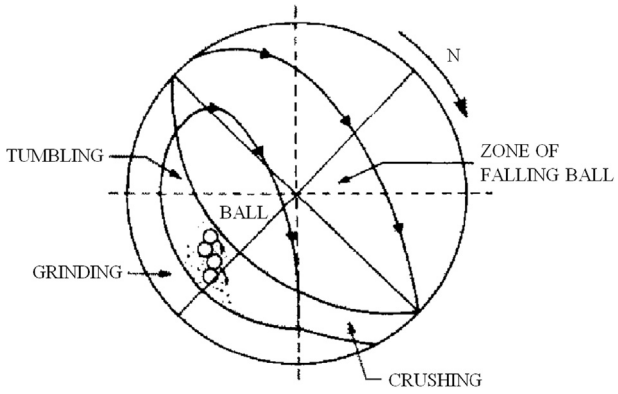

Fig. 8. Schematic illustration of comminution zones in a ball mill [28].

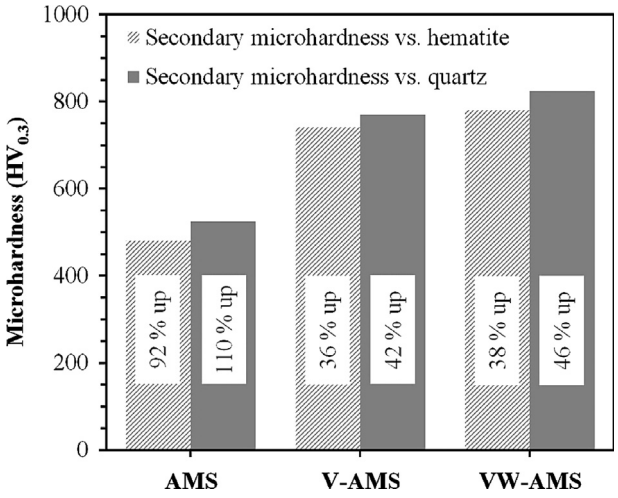

Fig. 9. Increase in the hardness of the austenite after BMAT.

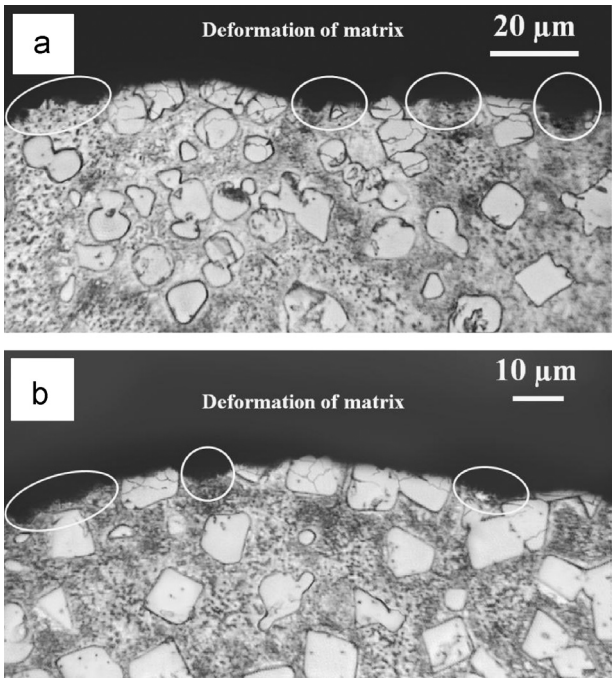

Fig. 10. Typical cross section of the composite materials after BMAT with (a) V-AMS vs. quartz and (b) VW-AMS vs. hematite minerals.

Altogether, microstructural studies demonstrated that predominant wear mechanism of the studied in-situ reinforced austenitic steel matrix composites was a combination of plastic deformation and micro-cutting of the matrix by abrasion along with microfracture of the reinforcements due to impact fatigue. Therefore, the remarkable increase in wear resistance of VW-AMS composite compared to the tungsten-free composite can be explained as follows: first, tungsten increased initial hardness and yield strength of the matrix. So, a better resistance to abrasion and plastic deformation was achieved. In addition, the worn surface of VW-AMS composite could be hardened more than W-free composite because of its higher work-hardening capacity (Table 2), making micro-cutting mechanism less effective. Secondly, in VW-AMS composite, vanadium carbides obtained higher strength, and the bonding at the interface of matrix with reinforcements was improved. Therefore, the applied load to the surface of material could be distributed more properly between the matrix and reinforcements. This could increase mechanical strength and ductility, simultaneously. It is evident in Table 2 where the specific work to fracture of the VW-AMS alloy (the area under stress–strain curve) was nearly 40% higher compared to V-AMS. Consequently, the wear rate was reduced as a considerable fraction of weight loss was likely to occur by fatigue under repeated impacts. However, compared to the previous findings [13], it can be concluded that by acquiring precise amount of tungsten addition to high-vanadium austenitic manganese steels, the beneficial effect of tungsten on enhancing the mechanical properties of the matrix and VC reinforcements can be achieved without the deleterious precipitation of W_3C phase in the structure. Finally, it was noticed that when the grinding media contained quartz, the in-situ reinforced composites offered relatively modest performance improvement compared to conventional austenitic manganese steel. In contrast, superior wear resistance of the composite materials was recognized in case of hematite. This key difference in performance of the studied austenitic matrix composite materials relative to the unreinforced austenitic manganese steel could be attributed to crushing strength (hardness) of the abrasive mineral which determines the high-stress or low-stress abrasion condition. The case where carbide reinforced materials showed markedly superior performance can be regarded as 'low-stress abrasion', and the case where carbides gave partial benefit can be regarded as 'high-stress abrasion'. Therefore, under high-stress abrasion condition, the cost-benefit balance seems likely to favor the low cost Hadfield steel in application demanding impact–abrasion resistance. While in low-stress condition, the situation is reversed and the in-situ reinforced austenitic matrix composite would be much more profitable for metal wastage and maintenance costs considerations in ore grinding and mineral processing industries.

4. Conclusions

The present paper reports the result of an investigation into the impact–abrasion wear characteristics of Fe–13Mn conventional austenitic steel, high-vanadium and tungsten-alloyed-high-vanadium Fe–13Mn austenitic steel matrix composites. Production of the in-situ VC-reinforced composite materials was quite feasible through conventional melting and casting route. The wear micromechanism of the matrix of the employed materials was plastic deformation of the austenite accompanied by subsurface impact–fatigue cracking of the reinforcements in case of in-situ reinforced composites. A noticeable increase in wear resistance of the composite materials was observed owing to the incorporation of VC particles in Fe-γ matrix. It was found that the W/V ratio increased from core to periphery of the particulates in VW-AMS

alloy due to diffusion of the dissolved tungsten from austenite into the growing vanadium carbides during solidification. This diffusion provided the VW-AMS composite with stronger particulates and improved interface bond of the matrix with the reinforcements leading to higher mechanical properties and wear performance compared to the tungsten-free composite material. It was observed that the relative performance of the synthesized in-situ composites in BMAT was strongly dependent on intrinsic characteristics of the abrasive minerals; the crushing strength (hardness) in particular. Consequently, when the grinding media contains strong minerals such as quartz, there may be no economical advantage from the use of sophisticated alloys such as particle-reinforced composite materials as they have unsatisfactory performance under high-stress impact abrasion. However, the presence of even modest proportions of softer mineral abrasives in working condition (i.e. low-stress abrasion condition), can alter the cost-benefit balance in favor of the regarding VC-reinforced composites with respect to conventional Hadfield steel.

Acknowledgments

The authors gratefully acknowledge the financial support of Tabarestan Steel Foundry Company (TSF Co.) and thank the Razi Metallurgical Research Center (RMRC) for giving assistances during all experimental works.

References

[1] T.S. Eyre, Tribol. Int. 9 (5) (1976) 203–212.
[2] D. Zhang, P.R. Beeley, A.J. Baker, Wear 173 (1994) 59–64.
[3] E. Bayraktar, C. Levaillant, S. Altintas, J. Mater. Process. Technol. 47 (1994) 13–31.
[4] S.A. Balogun, D.E. Esezobor, J.O. Agunsoye, J. Miner. Mater. Charact. Eng. 7 (3) (2008) 277–289.
[5] M. Abbasi, S. Kheirandish, Y. Kharrazi, J. Hejazi, Mater. Sci. Eng. A 513–514 (2009) 72–76.
[6] S. Aribo, K.K. Alaneme, D.O. Folorunso, F.O. Aramide, J. Miner. Mater. Charact. Eng. 9 (2) (2010) 157–164.
[7] J.R. Davis, Alloying: Understanding the Basics, ASM International, Ohio, 2001.
[8] H.S. Avery, M.J. Day, ASM Handbook vol. 1, Properties and Selection: Irons, Steels, and High-Performance Alloys, tenth ed., ASM International, Ohio, 1993.
[9] T.A. EL-Bitari, E.M. EL-Banna, Can. Metall. Q. 39 (3) (2000) 361–368.
[10] A. Sundstrom, J. Rendon, M. Olsson, Wear 250 (2001) 744–754.
[11] S.H. Mousavi Anijdan, A. Bahrami, N. Varahram, P. Davami, Mater. Sci. Eng. A 454–455 (2007) 623–628.
[12] E.G. Moghaddam, N. Varahram, P. Davami, Mater. Sci. Eng. A 532 (2012) 260–266.
[13] E.G. Moghaddam, N. Karimzadeh, N. Varahram, P. Davami, Metall. Mater. Trans. A 44 (2013) 3826–3835.
[14] I.R. Sare, Wear 87 (1983) 207–225.
[15] E. Albertin, A. Sinatora, Wear 250 (2001) 492–501.
[16] J.D. Gates, G.J. Gore, M.J.-P. Hermand, M.J.-P. Guerineau, P.B. Martin, J. Saad, Wear 263 (2007) 6–35.
[17] J.D. Gates, M.S. Dargusch, J.J. Walsh, S.L. Field, M.J.-P. Hermand, B.G. Delaup, J. R. Saad, Wear 265 (2008) 865–870.
[18] G.E. Dieter, Mechanical Metallurgy, SI metric ed, McGraw-Hill, London, 1988.
[19] S. Kuyucak, R. Zavadil, AFS Trans. 111 (2003) 1355–1369.
[20] ASM Handbook, vol. 3: Alloy Phase Diagrams, ASM International, Ohio, 1992.
[21] ⟨http://www.ptable.com⟩, 14.4.13.
[22] T.K. Bandyopadhyay, K. Das, J. Mater. Sci. 39 (2004) 6503–6508.
[23] L. Babout, Y. Brechet, E. Maire, R. Fougeres, Acta Mater. 52 (15) (2004) 4517–5425.
[24] R. Hadian, M. Emamy, N. Varahram, N. Nemati, Mater. Sci. Eng. A 490 (2008) 250–257.
[25] A.K. Srivastava, K. Das, Tribol. Int. 43 (2010) 944–950.
[26] C.E. Ridenourand, H.S. Avery, Canadian Pat. No. 894713, 1972.
[27] V.M. Kardonskii, O.V. Samoilova, Met. Sci. Heat Treat. 32 (8) (1990) 627–630.
[28] T. Ozben, E. Kilickap, O. Cakir, J. Mater. Process. Technol. 198 (2008) 220–225.
[29] P. Radziszewski, S. Tarasiewicz, Wear 160 (1993) 309–316.
[30] Y.N. Petro, V.G. Gavriljuk, H. Berns, F. Schmalt, Wear 260 (2006) 687–691.